

# Effects of B<sub>2</sub>O<sub>3</sub> and SiO<sub>2</sub> on dielectric properties and reliability of a lead-based relaxor dielectric ceramic

HIDEYUKI KANAI, OSAMU FURUKAWA\*, SHIN-ICHI NAKAMURA,  
YOHACHI YAMASHITA

*Toshiba Research and Development Center, Toshiba Corporation, 1 Komukai, Toshiba-cho, Saiwai-ku, Kawasaki 210 Japan*

The effects of B<sub>2</sub>O<sub>3</sub> and SiO<sub>2</sub> which are major constituents of vitreous low-firing agents on the dielectric properties and reliability of ceramic dielectrics were elucidated for the case of the lead-based relaxor dielectric ceramic [(Pb<sub>0.875</sub>Ba<sub>0.125</sub>)[Mg<sub>1/3</sub>Nb<sub>2/3</sub>]<sub>0.5</sub>(Zn<sub>1/3</sub>Nb<sub>2/3</sub>)<sub>0.3</sub>Ti<sub>0.2</sub>]<sub>0.3</sub>O<sub>3</sub>. Boron oxide (B<sub>2</sub>O<sub>3</sub>) led to a decrease in dielectric constant and degraded reliability under a humidity load condition at 85 °C and 95% RH. Although SiO<sub>2</sub> also caused a decrease in dielectric constant, it did not result in a reliability degradation. Analysis of the microstructure using TEM and STEM revealed that a water-soluble secondary phase consisting of B<sub>2</sub>O<sub>3</sub> and PbO was present at the grain boundaries and triple points in specimens with added B<sub>2</sub>O<sub>3</sub>. In contrast, no secondary phase existed in SiO<sub>2</sub>-doped specimens, but Si segregated at the grain boundaries. The existence of a water-soluble grain boundary phase was shown to degrade lifetime under humidity load conditions.

## 1. Introduction

Electronic components have been reduced in size as miniaturization has become the trend in electronic appliances. Among the miniaturized components playing a role in this trend, multilayer ceramic capacitors (MLCs) are typical examples; an MLC offers high capacitance in a small volume, as well as excellent lifetime performance. Conventionally, BaTiO<sub>3</sub>-based dielectrics have been used in MLCs. Since the sintering temperature must be higher than 1300 °C for such dielectrics, an expensive noble metal such as Pd has to be used for the electrodes. The inner electrodes account for approximately 60% of the total cost of such MLCs. For this reason, it has become commercially important to lower the sintering temperature in MLC production, thus allowing an inexpensive Ag/Pd system to be used instead. Recently, base metal systems such as Ni [1–4] and Cu [5] have been proposed as a replacement for Ag/Pd systems. However, if such base metal systems are used, the MLCs have to be fired in a reducing environment and at low temperature to suppress electrode oxidation. Therefore, using an Ag/Pd system for the internal electrodes is more practical in actual production. Of the several ways to achieve lower sintering temperatures, the use of glass to promote liquid-phase sintering is typical. Boron oxide [6, 7] and CuO [8] have been employed to lower the sintering temperature of BaTiO<sub>3</sub> and other dielectrics. Castellize *et al.* [7] found that the addition of up to 20 mol % of B<sub>2</sub>O<sub>3</sub> is effective in the case of

BaTiO<sub>3</sub>, lowering the sintering temperature and improving the mechanical properties and insulation resistance. It does, however, lower the dielectric constant. SiO<sub>2</sub> is also a popular constituent of glass. The effects of SiO<sub>2</sub> on dielectric properties and reliability have not yet been reported, however.

Recently PbO-based dielectrics called relaxors have been attracting attention because of their relatively low sintering temperatures and large dielectric constants. Relaxors are solid solutions of perovskite compounds such as Pb(Mg<sub>1/3</sub>Nb<sub>2/3</sub>)O<sub>3</sub>, Pb(Zn<sub>1/3</sub>Nb<sub>2/3</sub>)O<sub>3</sub>, and Pb(Fe<sub>1/2</sub>Nb<sub>1/2</sub>)O<sub>3</sub>. Yonezawa first developed these compounds and applied them as dielectrics in MLCs [9]. Since then, many dielectric compounds have been reported for use in MLCs [10–13]. One of the greatest advantages of using relaxors in MLC production is that inexpensive Ag/Pd inner electrodes can be utilized [8, 9]. However, there is a possibility of Ag migration into the dielectric layers of the MLC. This would lead to degradation of the insulation between dielectric layers, and could pose a very serious problem when the dielectric layer is reduced in thickness, such as to 6 μm. It is therefore necessary to suppress Ag migration by reducing the sintering temperatures. As practiced in BaTiO<sub>3</sub>-based MLC production, the addition of glass to dielectrics offers a practical means of lowering sintering temperature. However, the effects of SiO<sub>2</sub> and B<sub>2</sub>O<sub>3</sub>, the main components of the glass, on the dielectric properties and reliability of a relaxor have not been clarified. This paper looks into the

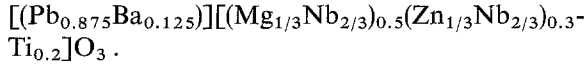
\* Present address: Electron Device Engineering Department, Toshiba Corporation, 8 Shin-sugita-cho, Isogo-ku, Yokohama, 235, Japan.

effects of  $B_2O_3$  and  $SiO_2$  on the dielectric properties and reliability of a relaxor.

## 2. Experimental details

### 2.1. Specimen preparation

The reference composition used in this experiment was the following:



The temperature coefficient of its dielectric constant ( $K$ ) satisfies the Y5U designation of the EIA standard [14]. Additives to the reference composition were  $B_2O_3$  and  $SiO_2$ . The amounts of addition were 100, 500, and 2000 p.p.m. Raw materials used throughout this experiment were reagent grade  $PbO$ ,  $BaCO_3$ ,  $MgCO_3$ ,  $Nb_2O_5$ ,  $ZnO$ , and  $TiO_2$ . Constituents were weighed, mixed in a ball-mill with water for 24 h, and then calcined in a closed alumina crucible at  $800^\circ C$  for 2 h. After the calcined powder was ball-milled with pure water and dried, 7 wt % of an aqueous solution containing 5 wt % of polyvinyl alcohol was added. The powder was granulated and pressed into 17 mm diameter, 1.5 mm thick disc pellets under 100 MPa of pressure. After binder burnout at  $600^\circ C$  for 10 min, the pellets were fired at  $1,050^\circ C$  for 2 h in a closed magnesia crucible.

### 2.2. Evaluation of dielectric

After firing, the density of the sintered material was measured by either the Archimedes method or by taking the dimensions. Grain size was measured by the intercept method on micrographs taken with a scanning electron microscope (SEM, Jeol T-20). Then, after polishing the disc specimens down to approximately 1 mm in thickness, electrodes 12 mm in diameter were formed on both faces using Ag paste. These printed electrodes were fired at  $700^\circ C$ . Dielectric properties were measured using an LF impedance analyser (YHP 4192A) at 1  $V_{rms}$  and 1 kHz. Resistivity was measured by applying 100 V to the specimens for one minute at room temperature and at  $125^\circ C$ . The phases formed were identified using the powder X-ray method with  $CuK_\alpha$  radiation, and the perovskite content was calculated using the following equation:

$$\text{Perovskite content (\%)} = \frac{100 \times I_{\text{pero.}(110)}}{I_{\text{pero.}(110)} + I_{\text{pyro.}(222)}}$$

where  $I_{\text{pero.}(110)}$  and  $I_{\text{pyro.}(222)}$  are, respectively, the intensities of the perovskite (110) reflection and the pyrochlore (222) reflection as determined through X-ray diffraction.

To carry out the reliability evaluation, fired disc specimens were polished down to 0.2 mm in thickness and Ag was evaporated on to both faces of the discs to form 10 mm diameter electrodes. Life test under a humidity load condition was conducted on these disc specimens at  $85^\circ C$  and 95% RH with an applied 700 d.c. voltage (which is approximately three times the rated voltage of an MLC).

The microstructure of specimens not subjected to humidity load condition was observed using a transmission electron microscope (TEM, Jeol 4000FX; Tokyo; Japan).

## 3. Results

### 3.1. Characterization of sintered specimens

Density was measured as a function of the additives. The density of the reference composition without additives was  $7.64 \text{ g cm}^{-3}$ , and this increased to  $7.82 \text{ g cm}^{-3}$  with the addition of up to 500 p.p.m. of  $B_2O_3$ . There was then a slight decrease upon the addition of 2000 p.p.m. of  $B_2O_3$ , as shown in Fig. 1. In contrast, the density of  $SiO_2$ -doped specimens decreased slightly.

The grain size in the reference specimen fired at  $1050^\circ C$  for 2 h was  $2.0 \mu\text{m}$ , as shown in Fig. 1. The addition of  $B_2O_3$  up to 500 p.p.m. caused a slight increase in grain size, but when 2000 p.p.m. was added it decreased. The grain size decreased with rising  $SiO_2$  concentration, reaching  $1.5 \mu\text{m}$  upon addition of 2000 p.p.m. of  $SiO_2$ .

It was noticed that the fracture mode varied with the type and quantity of additive. Fig. 2 shows how the ratio of transgranular area to total fracture area depends on the additive. In the reference specimen, 85% of the fracture surface was transgranular, while the specimen failed completely within the grains upon the addition of 500 p.p.m. of  $B_2O_3$ ; that is, the fracture mode was 100% transgranular. In contrast, the addition of  $SiO_2$  caused a change in fracture mode from transgranular to intergranular.

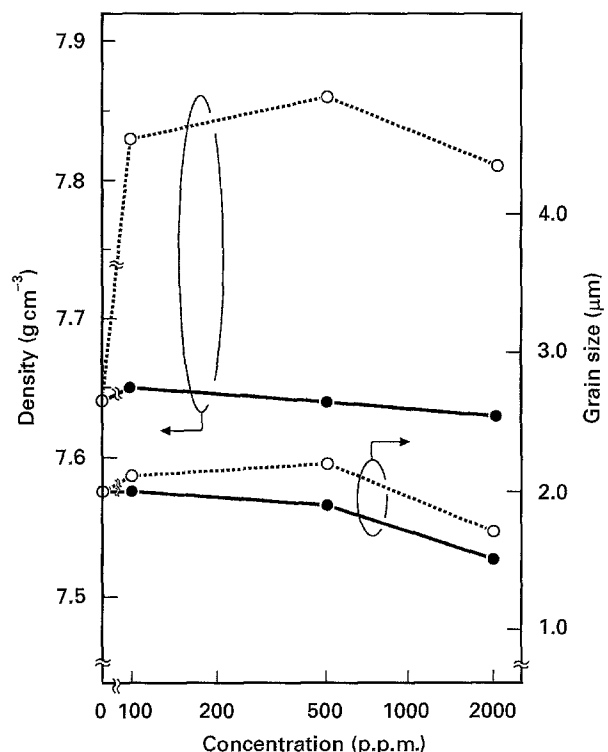


Figure 1 Effect of  $B_2O_3$  and  $SiO_2$  on density and grain size of specimens fired at  $1050^\circ C$  for 2 h. Key:  $\circ \dots \circ$   $B_2O_3$ ;  $\bullet \text{---} \bullet$   $SiO_2$ .

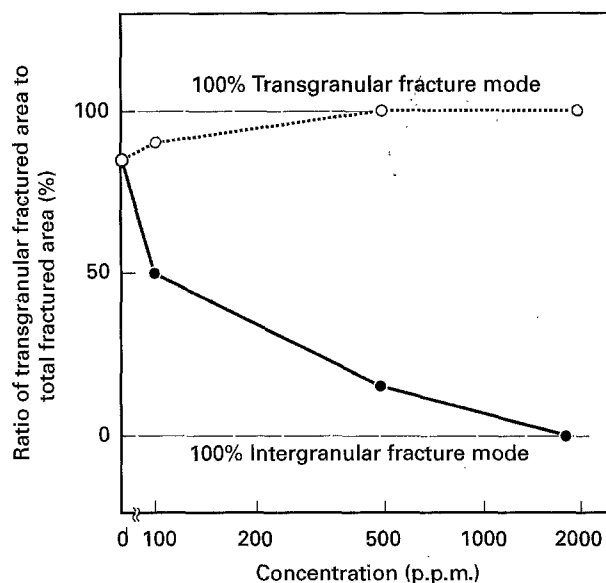


Figure 2 Effect of  $B_2O_3$  and  $SiO_2$  on the ratio of transgranular fracture area to total fracture area of specimens fired at  $1050^\circ C$  for 2 h. Key:  $\circ \dots \circ$   $B_2O_3$ ;  $\bullet \dots \bullet$   $SiO_2$ .

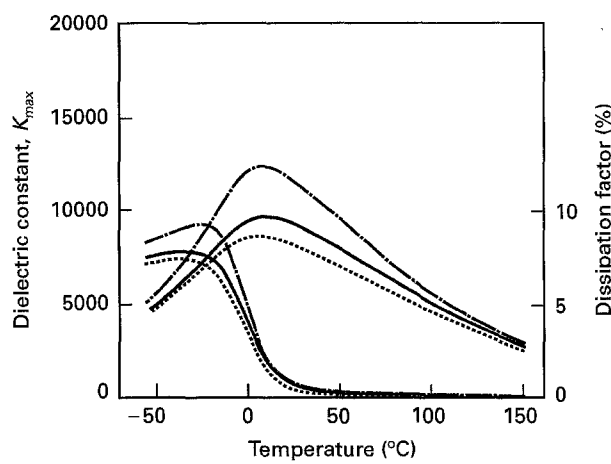


Figure 3 Effect of  $B_2O_3$  and  $SiO_2$  on the temperature coefficient of dielectric constant and dissipation factor. Key:  $\bullet \dots \bullet$  Reference;  $-\dots-$  2000 p.p.m.  $B_2O_3$ ;  $-\dots-$  2000 p.p.m.  $SiO_2$ .

### 3.2. Dielectric properties

Fig. 3 gives curves of the temperature coefficient of dielectric constant. Although the maximum dielectric constant,  $K_{max}$ , for the reference specimens was 12 100, it decreased with increasing concentration of  $B_2O_3$  and  $SiO_2$ .  $K_{max}$  was 9800 and 8800, for  $B_2O_3$  and  $SiO_2$ , respectively, at a concentration of 2000 p.p.m. This is shown in Fig. 4.

The dependence of Curie temperature ( $T_c$ ) on additive is shown in Fig. 4. The Curie temperature of the reference specimen was  $5^\circ C$ . However,  $T_c$  increased to  $10^\circ C$  with the addition of 2000 p.p.m. of  $SiO_2$ , while it did not change at all with the addition of  $B_2O_3$ .

### 3.3. Lifetime under a humidity load condition

The lifetime of specimens was measured under conditions of humidity loading. Fig. 5 shows the failure rate of 2000 p.p.m.  $B_2O_3$ -doped specimens and 2000 p.p.m.

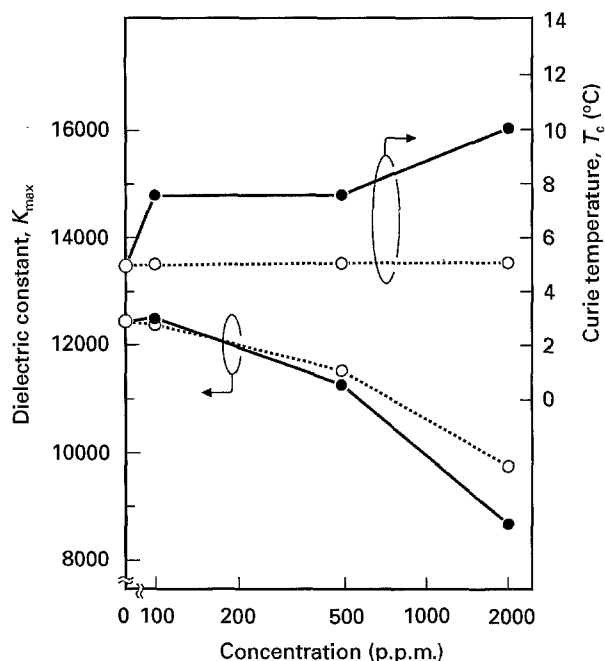


Figure 4 Effect of  $B_2O_3$  and  $SiO_2$  on maximum dielectric constant,  $K_{max}$ , and Curie temperature,  $T_c$ . Key:  $\circ \dots \circ$   $B_2O_3$ ;  $\bullet \dots \bullet$   $SiO_2$ .

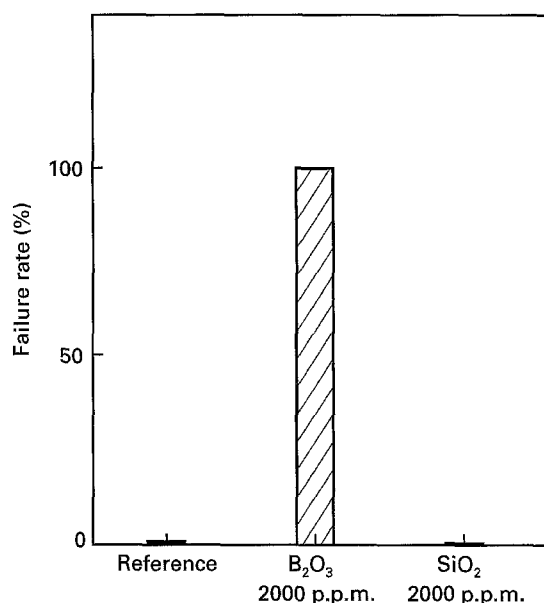


Figure 5 Effect of  $B_2O_3$  and  $SiO_2$  on failure rate after 500 h of humidity load test at  $85^\circ C$  and 95% RH with 700 V d.c. voltage (electrode diameter: 10 mm; specimen thickness: 300  $\mu m$ ).

$SiO_2$ -doped specimens. Although all the specimens doped with 2000 p.p.m. of  $B_2O_3$  degraded within 500 h, 2000 p.p.m.  $SiO_2$ -doped specimens and the reference specimens showed no degradation whatsoever.

## 4. Discussion

### 4.1. Microstructure analysis

Transmission electron microscope (TEM) observations and scanning transmission electron microscope (STEM) analysis were used to elucidate the respective roles of  $B_2O_3$  and  $SiO_2$  in determining dielectric characteristics and reliability. Fig. 6 shows

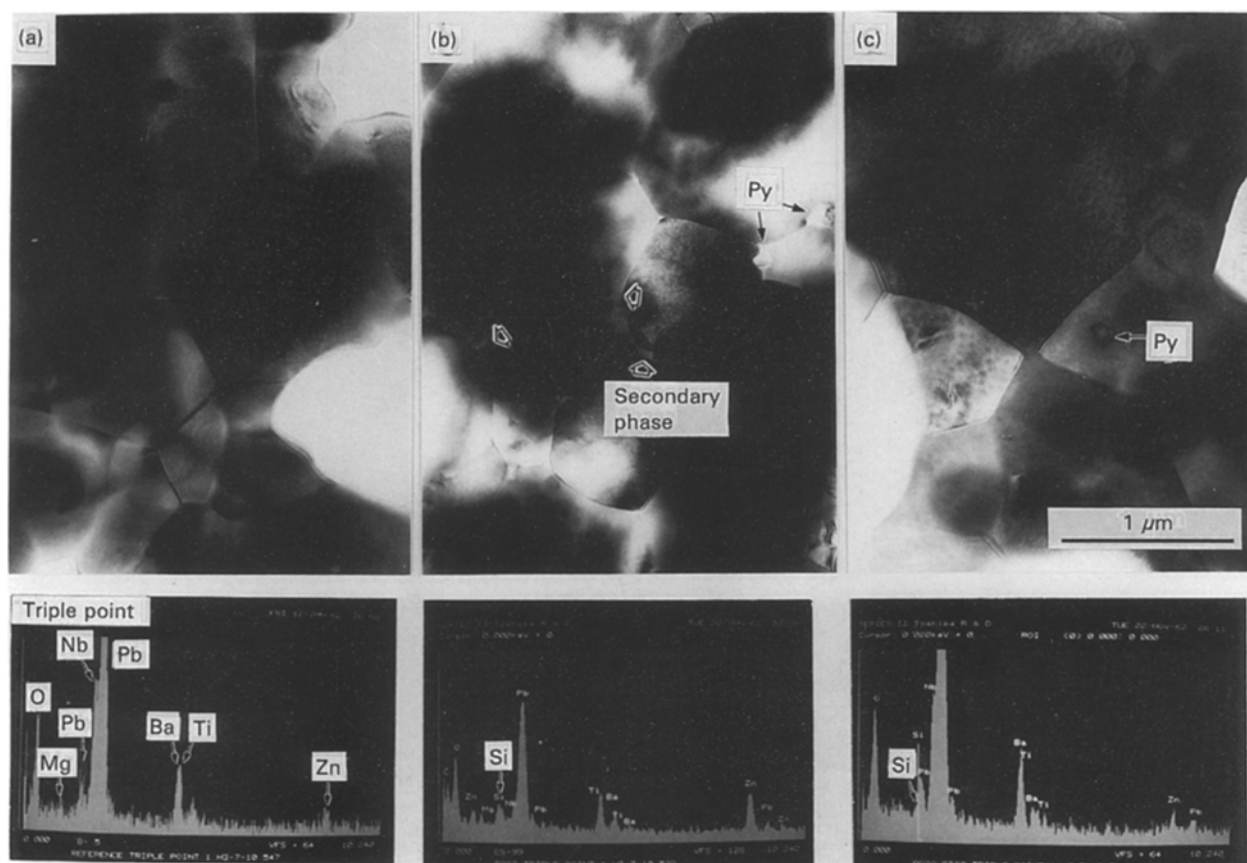


Figure 6 TEM micrographs of the reference specimen (a),  $B_2O_3$ -doped specimen (b), and the  $SiO_2$ -doped specimen (c).

TEM micrographs of specimens doped with these additives at the 2000 p.p.m. level. A secondary phase can be seen at the triple points and grain boundaries in the  $B_2O_3$ -doped specimen, while no secondary phase exists in the reference specimen. STEM analysis indicated large Pb signals in the secondary phase. However, no boron signal can be seen in the energy dispersive spectroscopy (EDS) spectra; this may be due to the poor sensitivity of EDS on STEM to trace amounts of light elements. The ionic radius of  $B^{3+}$  with a coordination number of 6 is 0.027 nm [15], making it too small to enter a B-site in the perovskite structure. As a consequence, boron probably segregates at the triple points and grain boundaries to form a secondary phase consisting of  $PbO-B_2O_3$ .

A TEM micrograph of an Si-doped specimen revealed the same microstructure as that of the reference specimen; no secondary phase was present at the triple points or grain boundaries. Silicon was detected at the triple points and grain boundaries.

#### 4.2. Role of $B_2O_3$

As shown in Fig. 1, the density of the specimens increased from the reference level with the addition of  $B_2O_3$ . Fig. 6 shows the secondary phase, which probably consists of  $B_2O_3-PbO$ . This phase might produce a liquid phase with a lower melting point, since the  $B_2O_3-PbO$  system can generate eutectic mixtures with melting points below  $770^\circ C$  [16]. Thus, the density of  $B_2O_3$ -doped specimens increased.

The maximum dielectric constant of  $B_2O_3$ -doped specimens was lower. There are two factors which affect  $K_{max}$ . One is the secondary phase formed at the grain boundaries. If the secondary phase, comprising  $PbO-B_2O_3$ , has a low dielectric constant ( $K$ ),  $K_{max}$  for bulk specimens will be much lower because a secondary phase with a low  $K$  value is present between the grains.

The second factor is the presence of a pyrochlore phase. Fig. 7 shows powder X-ray diffraction patterns for the reference and 2000 p.p.m.  $B_2O_3$ - and  $SiO_2$ -doped specimens fired at  $1050^\circ C$  for 2 h. Although the reference specimen indicates a 100% perovskite phase, analysis of the  $B_2O_3$ -doped specimen reveals a 4% pyrochlore phase. Since  $PbO$  is consumed in the formation of the secondary phase at the triple points and grain boundaries, the matrix composition changes from stoichiometric to  $PbO$ -deficient. As a result, the molar ratio of all elements at A sites in the perovskite structure to those at B sites, known as A/B, falls below 1.00, and the pyrochlore phase is formed.

It is well known that the dielectric constant decreases with falling grain size. However, increasing the amount of  $B_2O_3$  to 500 p.p.m. caused a decrease in  $K_{max}$  by 4% although there was no change in grain size. In addition, adding 2000 p.p.m. caused a great decrease (21%), even though the grain size decreased slightly. The decrease in  $K_{max}$  can therefore be mainly attributed to these two factors.

The fracture mode of the 2000 p.p.m.  $B_2O_3$ -doped specimen is 100% transgranular. This indicates that mechanically strong bonds form between the grains

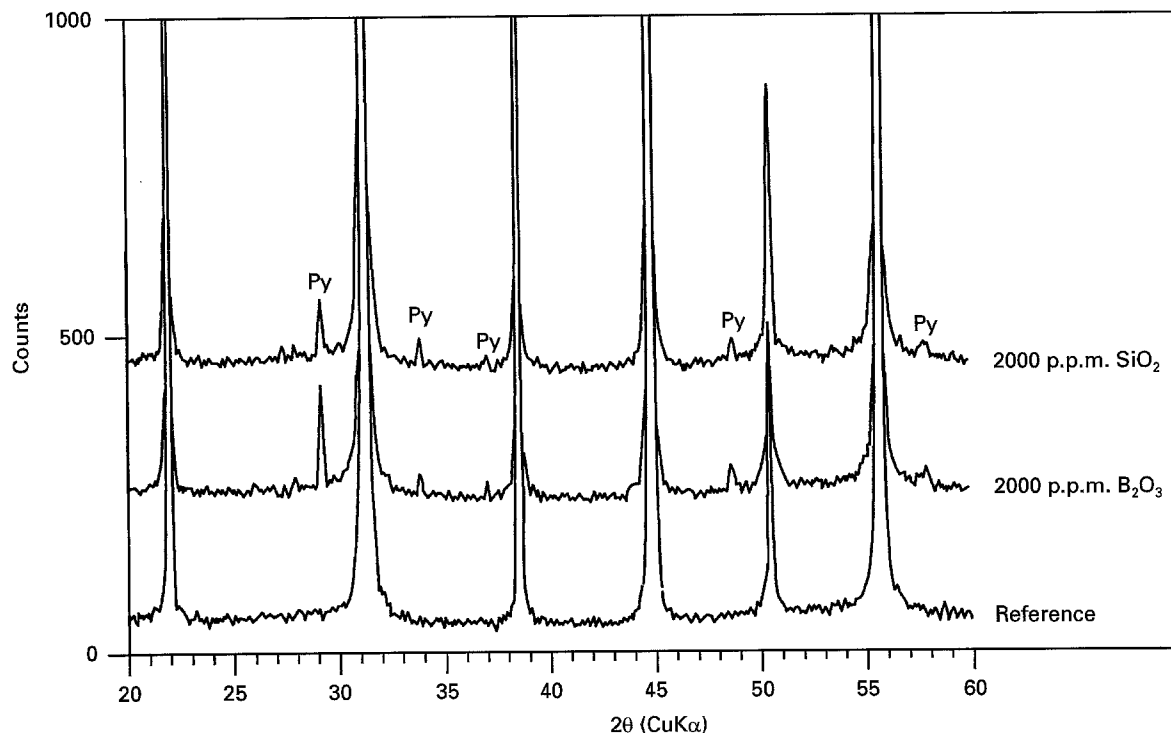


Figure 7 Powder X-ray diffraction patterns for the reference specimen,  $B_2O_3$ -doped specimen, and the  $SiO_2$ -doped specimen fired at  $1050^\circ C$  for 2 h.

due to the formation of the  $B_2O_3$ - $PbO$  grain boundary phase. However, this grain boundary phase is very vulnerable to humid conditions, since  $PbO$  and  $B_2O_3$  are slightly soluble in water [17]. When compared with the reference specimen,  $B_2O_3$ -doped specimens suffered rapid degradation via the degradation mechanism proposed earlier by the authors [18].

#### 4.3. Role of $SiO_2$

A small amount of Si was detected at triple points and grain boundaries. The ionic radius of  $Si^{4+}$ , which has a coordination number of 6, is 0.04 nm [15]. Taking this into account, there are two possibilities: either Si enters B sites in the perovskite structure, or some of the Si segregates at the grain boundaries. As shown in Fig. 4,  $T_c$  increased by  $5^\circ C$  with the addition of 2000 p.p.m. of  $SiO_2$ , indicating that dissolution of Si into B sites in the perovskite structure takes place. The resulting fall in  $A/B$  to less than 1.00 causes the pyrochlore phase to be formed, as shown in Fig. 7. The grain size in  $SiO_2$ -doped specimens is smaller than that in the reference specimen. The segregation of  $SiO_2$  at the grain boundaries prevents grain growth, and also alters the fracture mode from transgranular to intergranular. When compared with  $B_2O_3$ -doped specimens, the decrease in  $K_{max}$  is more significant. Therefore, three factors mentioned above, segregation of Si at grain boundaries, formation of pyrochlore phase, and small grain size, may be responsible for the decrease in  $K_{max}$  in Fig. 4.

Under humidity load conditions, the presence of a water-soluble secondary phase or segregated material at the grain boundaries degrades the lifetime of dielectrics [18]. The reason for the excellent life-

time performance of  $SiO_2$ -doped specimens under humidity loading is that the  $SiO_2$  which segregates at the grain boundaries is insoluble in water.

#### 5. Conclusion

The effects of using  $B_2O_3$  and  $SiO_2$  as the major constituents of vitreous low-firing agents were investigated as a function of dielectric properties and reliability. As regards the use of lead-based relaxor dielectric ceramics in MLCs, it is concluded that in using glass as an additive, it should contain a minimum of  $B_2O_3$  so as to prevent reliability degradation under humidity load conditions as well as to ensure that the dielectric constant is not reduced. Since  $SiO_2$  causes a decrease in dielectric constant, addition of glass containing  $SiO_2$  should be avoided when attempting to lower the firing temperature.

#### References

1. J. M. HERBERT, *Trans. Brit. Ceram. Soc.* **62** (1963) 645.
2. I. BURN and G. M. MAHER, *J. Mater. Sci.* **10** (1975) 633.
3. H. J. HAGEMAN and D. HENNINGS, *J. Amer. Ceram. Soc.* **64** (1981) 590.
4. Y. SAKABE, K. MINAI and K. WAKINO, *Jpn. J. Appl. Phys. Suppl.* **20-4** (1981) 147.
5. J. KATO, Y. YOKOTANI, H. KAGATA and H. NIWA *Jpn. J. Appl. Phys. Suppl.* **26-2** (1987) 90.
6. I. BURN, *J. Mater. Sci.* **17** (1982) 1398.
7. L. M. CASTELLIZE and R. J. ROUTIL, *J. Can. Ceram. Soc.* **35** (1969) 69.
8. D. HENNINGS, *Ber. Dtsch. Keram. Ges.* **55** (1978) 359.
9. M. YONEZAWA, *Bull. Amer. Ceram. Soc.* **62** (1984) 1375.
10. J. M. MAHER, in Proceedings of the 27th Electronic Components Conference (IEEE, 1977) pp. 391-399.

11. M. YONEZAWA, K. UTSUMI and T. OHNO, in Proceedings of the 1st Meeting on Ferroelectrics and Their Application (1977) p. 297.
12. K. FURUKAWA, S. FUJIWARA and T. OGASAWARA, in Proceedings of the Japan-U.S. Study Seminar on Dielectrics and Piezoelectric Ceramics (1982) p. T-4.
13. J. KATO, Y. YOKOTANI, M. NISHIDA, S. KAWASHIMA and H. OUCHI, *Jpn. J. Appl. Phys. Suppl.* **24-3** (1985) 90.
14. O. FURUKAWA, M. HARATA, Y. YAMASHITA, K. INAGAKI and S. MUKAEDA, *Jpn. J. Appl. Phys.* **26** (1987) 34.
15. R. D. SHANNON, *Acta Crystallogr.* **A32** (1976) 751.
16. E. M. LEVIN, C. R. ROBBINS and H. F. McMURDIE, "Phase Diagrams for Ceramics" (The American Ceramic Society, Columbus, OH, 1964).
17. J. W. MELLOR, "A Comprehensive Treatise on Inorganic and Theoretical Chemistry" Vol. 7 (Longmans, Green and Co. Ltd., London, 1927).
18. H. KANAI, O. FURUKAWA, S. NAKAMURA and Y. YAMASHITA, *J. Amer. Ceram. Soc.* **76** (1993) 459.

*Received 10 May 1994  
and accepted 4 October 1995*